Supporting Information

Predicting Hazardous Sb(III)/Sb(V) Adsorption on Biochar via An Interpretable ML-DFT Integrated BiMeSorb Framework with Experimental Validation

Yaoshuo Zhang[a, #], Chenxi Zha[a, #], Lijie Yuan[a, #], Yanzhong Li[a], Yinan Dong[b], Dongli Li[b], Ludong Yi[b], Zehui Li[b, c, d *], Shengbing He[b, c], Dongyang Li[a, *]

[a] School of Chemical Engineering, Zhengzhou University, Zhengzhou 450001, China.

[b] National Observation and Research Station of Erhai Lake Ecosystem in Yunnan, School of Environmental Science and Engineering, Shanghai Jiao Tong University, Shanghai 200240, China

[c] Shanghai Jiao Tong University Yunnan Dali Research Institute, Dali 671000, P. R. China

[d] Shanghai Engineering Research Center of Solid Waste Treatment and Resource Recovery, Shanghai Jiao Tong University, Shanghai 200240, China

[#] These authors contributed equally

[*] Corresponding author: Zehui Li, Dongyang Li

Email address: zehuili@sjtu.edu.cn, dyli@zzu.edu.cn

Table S1. Comparison of methodological features between this work and previously reported machine learning studies on biochar adsorption systems

Contaminant	Multi-species ML	Dataset Size	Test R^2	Mechanistic Level	Experimental	Study
Phosphorus	—	1200	0.893	PDP	—	(Lyu et al., 2024)
Phosphate	—	163	0.98	SHAP+PDP+ experiment	✓	(Fu et al., 2025)
Fluoride	—	576	0.922	SHAP+PDP+ experiment	✓	(Fan et al., 2025)
Sb and other emerging contaminants	✓	528	0.94	SHAP+PDP	—	(Ullah et al., 2025)
Sb(III)/Sb(V) As(III)/As(V)	—	—	—	Experiment	✓	(Wei et al., 2024)
Sb(III)	—	—	—	Experiment+ DFT	✓	(Chen et al., 2024)
Sb(III)/Sb(V)	✓	474	0.934	SHAP+PDP+ experiment + DFT	✓	This work

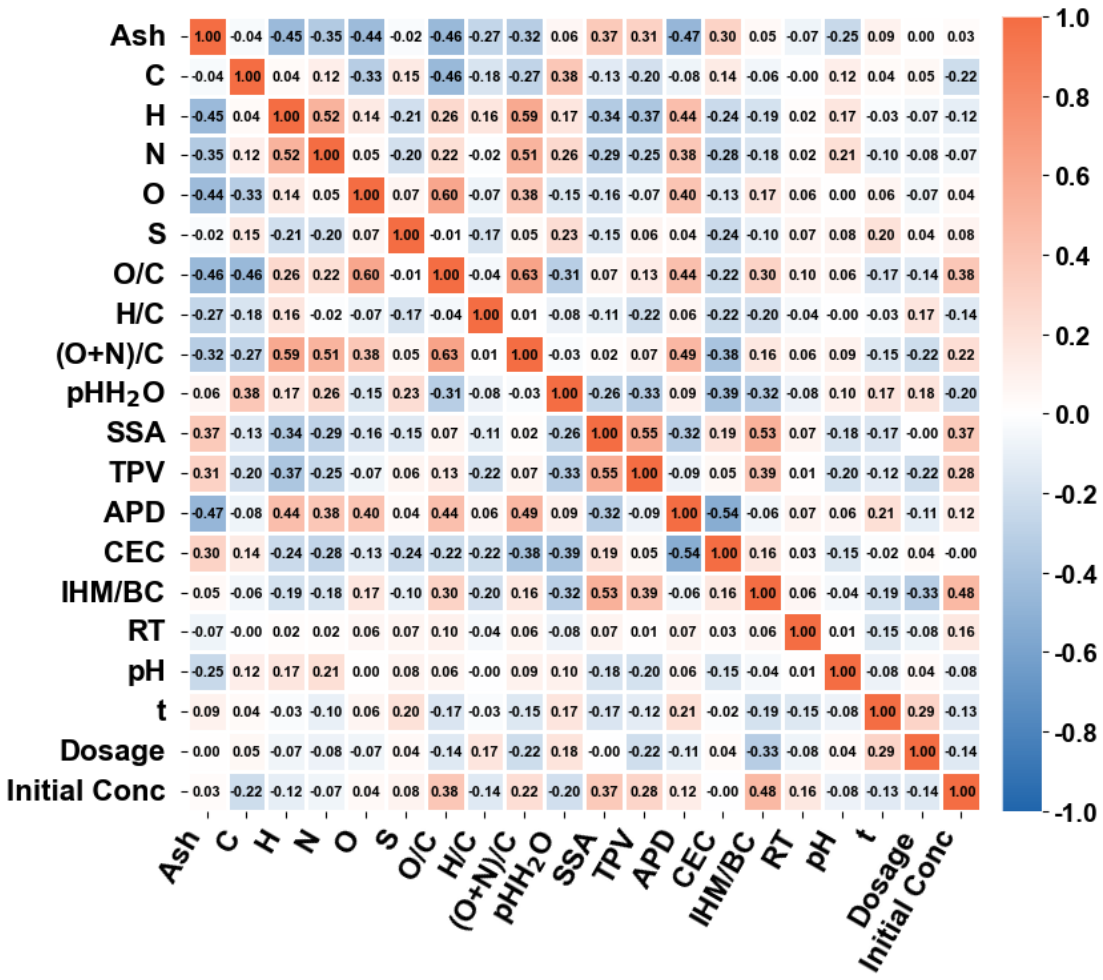

Figure S1. Heatmap of Pearson correlation coefficients among the input numerical features.

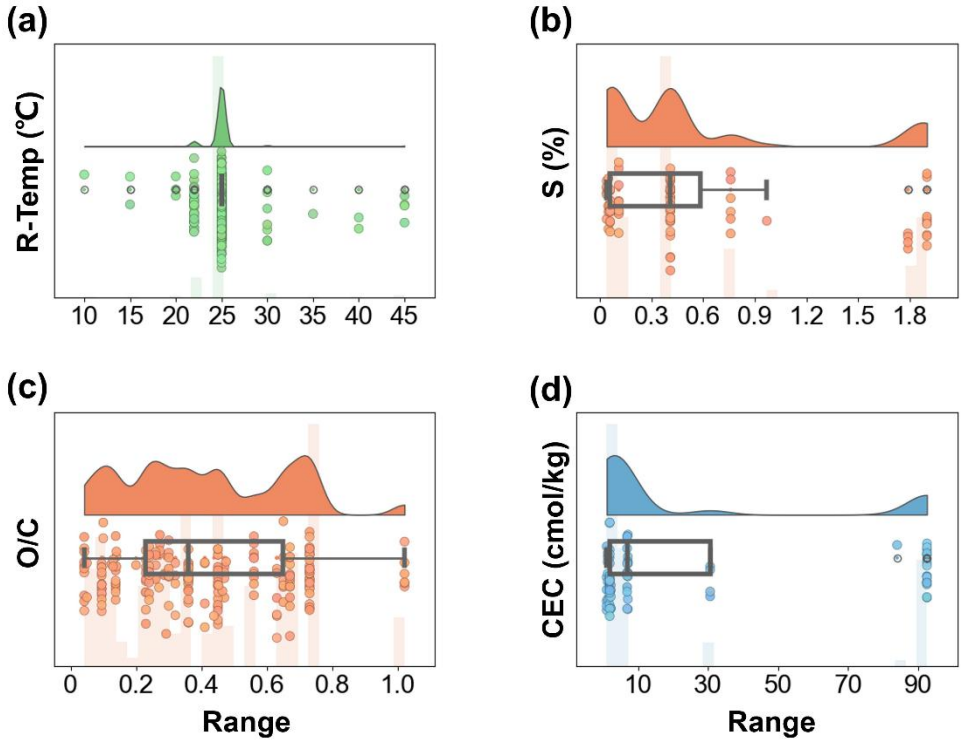

Figure S2. Scatter–raincloud plots showing the data distributions of the four input features considered for removal after analysis.

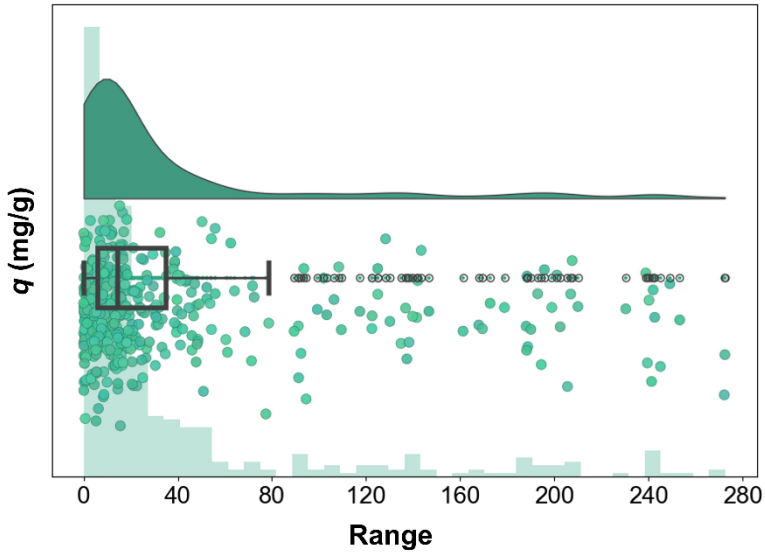

Figure S3. Raincloud plot illustrating the data distribution of the output feature.

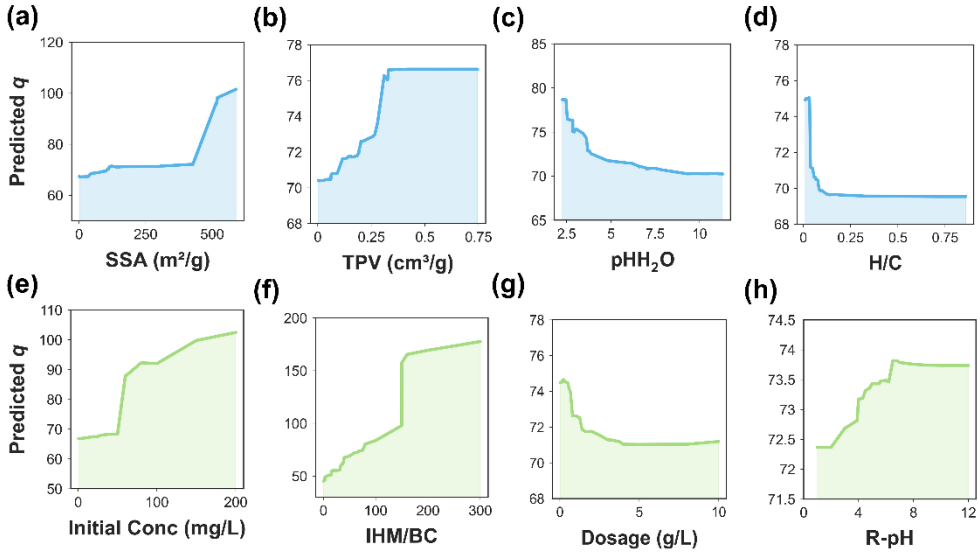

Figure S4. Partial dependence analyses of the most influential variables using the RF model.

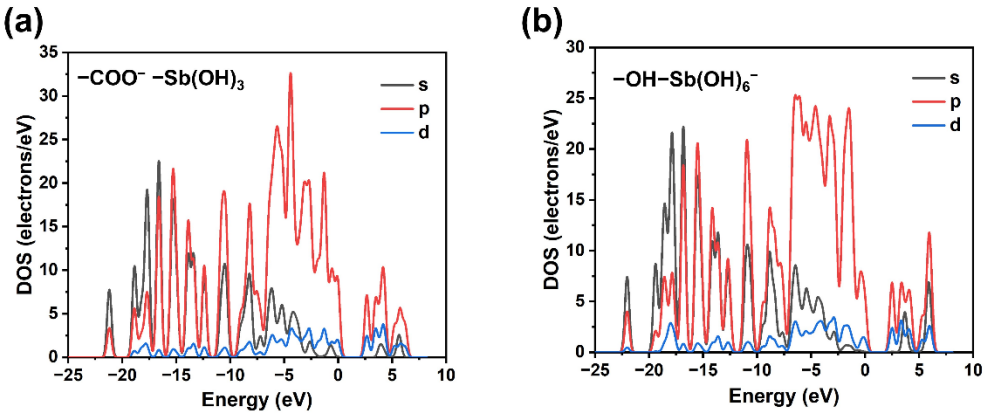

Figure S5. Projected density of states (PDOS) of the dominant Sb adsorption configurations: (a) −COO⁻–Sb(OH)$_3$ and (b) −OH–Sb(OH)$_6^-$. Black, red, and blue curves represent the contributions from s, p, and d orbitals, respectively, with the p states mainly arising from O 2p and Sb 5p orbitals and the d states primarily contributed by Sb.

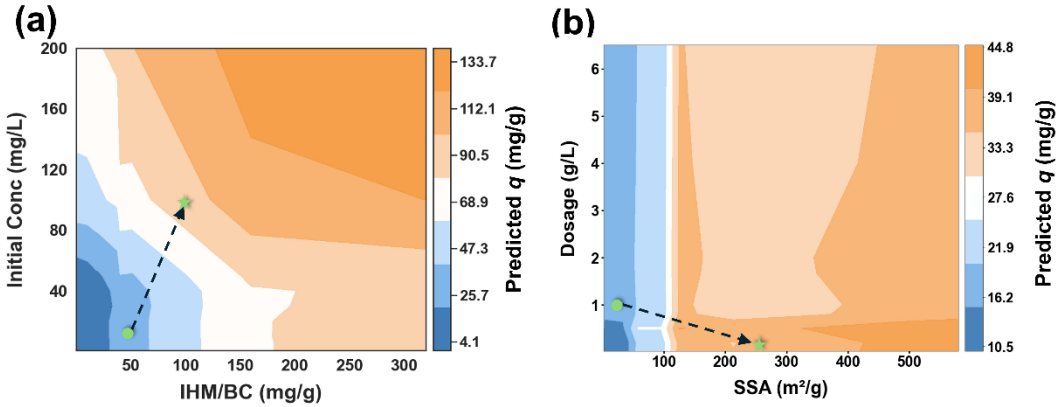

Figure S6. Verification of the predictive model for Sb removal: Consistency between observed experimental trends and coupled interaction response patterns.

Table S2. Six supporting studies were used to validate the reliability of the model. The following entries summarize the optimal adsorbent conditions and the corresponding experimental parameters reported in these references.

Ref	SSA	IHM/BC	C_0	m	q
(Yang et al., 2025)	55.64	200	200	1	237.26
(Chen et al., 2025)	70.77	227.27	200	0.88	142.6
(Liu et al., 2022)	124.04	310	155	0.5	117.75
(Huang et al., 2024)	272.1	200	50	0.25	180.74
(Deng et al., 2025)	146.2	40	20	0.5	20.3
(Fang et al., 2025)	415.58	6.67	10	1.5	151.5

References

Chen H, Gao Y, Fang Z, Li J, Pillai S C, Song H, Sun C, Bolan N, Yang X, Vithanage M, Shan S, Wang H (2024). Investigating the electron-scale adsorption mechanisms using DFT calculations and experimental studies in self-assembly magnetic biochar gel incorporated with graphene nanosheets for enhanced Sb(III) removal. Chemical Engineering Journal, 487: 150740

Chen Y, Yang W, Liu H, Wu Y, Yu Y, Zhang J, Wang B, Yang L, Wang S, Zhou H, Wu P (2025). Acid mine drainage sludge as an iron source modified biochar for Sb(III/V) removal: Mechanisms and adsorption behavior with As(III). Journal of Environmental Chemical Engineering, 13(5): 118163

Deng S, Ren B, Cheng S, Hou B, Deng R, Zhu G (2025). Study on the adsorption performance of carbon-magnetic modified sepiolite nanocomposite for Sb(V), Cd(II),

Pb(II), and Zn(II): Optimal conditions, mechanisms, and practical applications in mining areas. Journal of Hazardous Materials, 487: 137129

Fan L, Wang D, Yu H, Gong Z, He Y, Guo J (2025). Application of machine learning to predict the fluoride removal capability of MgO. Journal of Environmental Chemical Engineering, 13(1): 115317

Fang R, Peng J, Yu L, Wang Z, Pan K, Yan C, Zhou S (2025). Fast preparation of high-performance zero-valent iron biochar materials for the removal of arsenic and antimony pollutants utilizing waste wheat straws. Carbon Neutrality, 4(1): 14

Fu W, Yao X, Zhang L, Zhou J, Zhang X, Yuan T, Lv S, Yang P, Fu K, Huo Y, Wang F (2025). Design optimization of bimetal-modified biochar for enhanced phosphate removal performance in livestock wastewater using machine learning. Bioresource Technology, 418: 131898

Huang W, Yang Z, Hu J, Chen X, Li W, Wang Z, Zhang C, Wang Q, Xiao X, Yu P (2024). Mechanisms and valorization of selective adsorption of Sb(III) by amino-functionalized lignin-based porous biochar. Chemical Engineering Journal, 499: 156262

Liu J, Wei X, Ren S, Qi J, Cao J, Wang J, Wan Y, Liu Y, Zhao M, Wang L, Xiao T (2022). Synergetic removal of thallium and antimony from wastewater with jacobsite-biochar-persulfate system. Environmental Pollution, 304: 119196

Lyu H, Xu Z, Zhong J, Gao W, Liu J, Duan M (2024). Machine learning-driven prediction of phosphorus adsorption capacity of biochar: Insights for adsorbent design and process optimization. Journal of Environmental Management, 369: 122405

Ullah H, Khan S, Zhu X, Chen B, Rao Z, Wu N, Idris A M (2025). Machine learning-aided biochar design for the adsorptive removal of emerging inorganic pollutants in water. Separation and Purification Technology, 362: 131421

Wei M, Wang B, Wu P, Zhang X, Chen M, Wang S (2024). Electrolytic manganese residue-biochar composite for simultaneous removal of antimony and arsenic from water: Adsorption performance and mechanisms. Journal of Cleaner Production, 437: 140623

Yang X, Yu J, Liu Y, Duan R, Tang Q, Tian L, Xu R, Wang H, Xiang T (2025). Lead and antimony removal from wastewater via tea residue derived hydrochar: Immobilization capacity and industrial practicality. Industrial Crops and Products, 231: 121158